Desalination 619 (2026) 119572

Contents lists available at ScienceDirect

Desalination

journal homepage: www.elsevier.com/locate/desal

Enhancing water recovery in reverse osmosis by mitigating membrane scaling using thermomorphic hydrophilicity base-induced precipitation pretreatment

Yuren Feng [a], Sara Abu-Obaid [a], Daniel Galperin [a], Ngai Yin Yip [a,b,*]

[a] Department of Earth and Environmental Engineering, Columbia University, New York, NY, 10027-6623, United States
[b] Columbia Water Center, Columbia University, New York, NY, 10027-6623, United States

HIGHLIGHTS

- THBIP pretreatment mitigates scaling by removing hardness cations Ca^{2+} and Mg^{2+}.
- Flux decline rate due to initial gypsum scaling was reduced by 14.7 % relative to untreated feed.
- THBIP suppressed anhydrite formation, extending productivity window from 0.48 to 0.61 in water recovery yield.

ARTICLE INFO

Keywords:
Membrane scaling mitigation
Thermomorphic Hydrophilicity Base-Induced Precipitation (THBIP) pretreatment
Hardness removal
Enhanced water recovery
Mineral precipitation
Reverse osmosis
Desalination

ABSTRACT

Membrane scaling remains one of the primary operating challenges in reverse osmosis (RO) desalination, especially for feedwaters with high scaling potential. The conventional mitigation approach of antiscalant dosing provides only temporary relief by delaying nucleation but adds cost and complexity, introduces other fouling risks, and leaves the underlying supersaturation of hardness ions, i.e., Ca^{2+} and Mg^{2+}, unaddressed. This study investigates thermomorphic hydrophilicity base-induced precipitation (THBIP), a thermomorphic solvent-based emerging descaling technique, as an alternative pretreatment for scaling mitigation by selectively removing hardness cations from the feed. Bench-scale crossflow RO experiments using high-scaling propensity feed simulating irrigation drainage water demonstrated that THBIP pretreatment significantly reduced the rate of water flux decay by 14.7 % compared to untreated feed. THBIP-pretreatment extended the water recovery yield from 0.48 to 0.61 before severe scaling occurred, representing a 27 % productivity gain over the control. Whereas the untreated feed experienced catastrophic flux collapse shortly after the critical transition point, THBIP-pretreated membranes retained ≈61–66 % of their initial water permeability. Integrated thermodynamic, morphological, elemental, and crystallographic analyses revealed that initial scaling was driven by gypsum, whereas the critical transition was triggered by the subsequent onset of anhydrite precipitation. By suppressing anhydrite formation, which forms denser, less permeable deposits than gypsum, THBIP drastically reduced the flux decline rate by 71.7 % relative to the controls while preserving salt rejection. With the intrinsic advantages of chemical recyclability, feed pH rebalancing, and compatibility with low-grade heat utilization, THBIP offers a more effective and sustainable solution for managing high-scaling RO feeds.

1. Introduction

Global water scarcity is an increasingly pressing issue, with nearly two-thirds of the world's population projected to face water stress by 2050 [1–4]. Given that only 0.014 % of Earth's water is readily accessible as freshwater, alternative water supplies are increasingly vital [3,5]. Seawater and brackish water desalination have emerged as critical components of sustainable water solutions worldwide [6]. Among available desalination methods, membrane-based reverse osmosis (RO) has emerged as the dominant technology and market leader, accounting for the majority of global desalination capacity due to its high separation efficiency and lower energy requirements compared to distillation

* Corresponding author at: Department of Earth and Environmental Engineering, Columbia University, New York, NY, 10027-6623, United States.
E-mail address: n.y.yip@columbia.edu (N.Y. Yip).

https://doi.org/10.1016/j.desal.2025.119572
Received 30 August 2025; Received in revised form 27 October 2025; Accepted 27 October 2025
Available online 30 October 2025

[7–10].

RO operates through pressure-driven transport of water across semi-permeable membranes while rejecting dissolved salts and contaminants [11–15]. However, mineral scaling of the membrane remains a principal operational challenge, constraining process efficiency and economic viability [16–18]. Scaling occurs when sparingly soluble minerals, e.g., calcite (calcium carbonate, $CaCO_3$), gypsum (calcium sulfate dihydrate, $CaSO_4 \bullet 2H_2O$), brucite (magnesium hydroxide, $Mg(OH)_2$), and silica (SiO_2), exceed their respective solubility thresholds, leading to precipitation of crystalline salts (Ca/Mg) or polymerization of amorphous deposits (silica) on the membrane surface [16,19–21]. These deposits gradually build up a dense fouling layer that progressively hinders water transport, reducing permeate flux, increasing transmembrane pressure requirements, elevating energy consumption, and necessitating frequent chemical cleaning cycles (clean-in-place). The technical difficulties caused by mineral scaling collectively compromise the economic feasibility and environmental sustainability of RO operations, especially for feeds with high scaling potential [11,16,19].

Current scaling mitigation strategies rely mainly on chemical approaches, such as antiscalant dosing, to maintain supersaturated species below critical nucleation thresholds or disturb ordered crystal growth [11,22–26]. While the introduction of antiscalants can delay scale formation or inhibit regular crystalline structures, they inevitably increase process complexity and operating costs. Anti-scaling chemicals, typically phosphonate (PO_3^{2-}) or polycarboxylate-based ($[C_nH_{2n+1}COO]_n$) compounds, require precise dosing control, may contribute to organic and biochemical fouling, and are less effective for feedwaters with high scaling propensity [21,27–29]. More importantly, using complexing agents to chelate the scaling precursor ions can only provide temporary relief as the underlying driver for precipitation remains, with hardness ions such as Ca^{2+} and Mg^{2+} persisting in the feed stream. Consequently, antiscalants become increasingly inefficient as scaling kinetics intensify with increasing water recovery yields, limiting the practical operating range of RO [22,27]. Inter-stage concentrate demineralization approaches that include chemical precipitation, ion exchange, and intermediate nanofiltration, have been studied to improve RO water recovery yields, but have associated operational complexity and waste disposal challenges [30–32]. Conventional ICD methods typically result in 10–20 % recovery improvements but have certain limitations: lime precipitation involves high chemical use and generates large amounts of sludge; ion exchange systems require frequent regeneration, leading to waste brines; nanofiltration increases capital and energy requirements. Each method has associated operational complexity and challenges regarding waste disposal.

Thermomorphic hydrophilicity base-induced precipitation (THBIP) is an alternative pretreatment approach that has been demonstrated for descaling hypersaline brines [33]. Detailed working principles can be found in initial study [33]. Briefly, the technique employs thermosensitive amine bases that undergo reversible hydrophilic-hydrophobic transitions. In the hydrophilic state at ambient temperatures, the basic amines dissolve in water and increase the solution pH to initiate the precipitation of hardness cations in hydroxide forms. The high thermal sensitivity enables subsequent amine recovery: toggling the amine to its hydrophobic state through the application of a mild thermal stimulus drives temperature-induced phase separation, allowing for amine regeneration. Significant Ca^{2+} and Mg^{2+} removals of >33 % and >90 % as $Ca(OH)_{2(s)}$ and $Mg(OH)_{2(s)}$, respectively, were achieved from a high background of 233.8 g/L NaCl (4.0 mol/L) by raising the pH to ≈12.2 using diisopropylamine [33]. Importantly, the amine does not react directly to form the solid precipitates, i.e., the process is non-consumptive. Amine recyclability is enabled by the thermomorphic multiphase nature of the system: the drastic decrease of amine solubility in water at moderate temperature increases allows simple thermal-induced phase separation of the organic amines from aqueous saline feed to achieve amine regeneration. Critically, this recovery process concurrently lowers the feed pH, eliminating the need for additional pH adjustment prior to subsequent cycles—a significant advantage over conventional hydroxide and other base dosing strategies that permanently elevate pH [34,35]. While the innovation has been demonstrated for descaling hard brines, the actual benefits of utilizing THBIP as a pretreatment for RO have not been quantitatively examined.

This study investigates the performance improvements of thermomorphic hydrophilicity base-induced precipitation pretreatment on reverse osmosis desalination of a high-scaling propensity feed. Water recovery yield and salt rejection were evaluated for the RO desalination of untreated and THBIP-pretreated feeds simulating brackish irrigation drainage water in the San Joaquin Valley (CA, United States), and mineral scaling was assessed by quantifying the water flux decline. Water chemistry analysis was combined with morphological and X-ray spectroscopic characterizations of the scalant to explain the role of different mineral precipitates and the mechanism of water recovery improvement by THBIP. Lastly, the implications of thermomorphic solvent-based THBIP as a potential pretreatment for high-scaling propensity RO feeds are discussed.

2. Material and methods

2.1. Materials

RO feedwater was prepared using ACS-grade or higher purity chemicals. Sodium bicarbonate ($NaHCO_3$, >99 %) and magnesium chloride hexahydrate ($MgCl_2 \cdot 6H_2O$, >99 %) were procured from Thermo Scientific (Waltham, MA, United States). Calcium chloride dihydrate ($CaCl_2 \cdot 2H_2O$, >99 %), sodium sulfate (Na_2SO_4, >99 %), and ammonium chloride (NH_4Cl, >99 %) were acquired from Acros Organics (Waltham, MA, United States). Sodium chloride (NaCl, >99 %) was obtained from Alfa Aesar (Haverhill, MA, United States), and sodium nitrate ($NaNO_3$, >99 %) from Sigma-Aldrich (St. Louis, MO, United States). All chemicals were used as received without further modification. Commercial Filmtec BW-30 RO membranes (DuPont, Wilmington, DE, United States) were used in all RO experiments. Permeate flow rates were measured using a precision balance (Adventurer, OHAUS, Parsippany, NJ, United States) in conjunction with a high-performance liquid chromatography-grade digital liquid flowmeter (GJC Instruments Ltd., Chester, United Kingdom). Deionized (DI) water was obtained from a Milli-Q ultrapure water purification system (Millipore, Billerica, MA, United States).

2.2. Assessment of hardness change on water recovery and salt rejection of reverse osmosis

Membrane coupons were cut to 6 cm × 10 cm and conditioned through sequential soaking in isopropyl alcohol for 2 h followed by DI water for 24 h to remove residual manufacturing chemicals (e.g., preservatives) and achieve complete membrane wetting. Conditioned membranes were subsequently installed into five RO test cells with active membrane area of 19.4 cm^2 each (25.4 mm by 76.2 mm) and compacted by circulating 4 L of DI water at 27.6 bar (400 psi) with crossflow velocity of 0.11 m/s for 24 h to establish stable baseline permeability.

Appropriate amounts of concentrated cation (as chloride salts) and anion (as sodium salts) stock solutions were carefully added into the feed reservoir containing DI water and thoroughly mixed by circulation to constitute the RO feeds for assessing scaling mitigation efficacy of THBIP pretreatment. The control feed solution was formulated to replicate the composition of feedwater at the San Luis RO Plant, which desalinates irrigation drainage water from San Joaquin Valley, CA, United States, i.e., without pretreatment. To prevent premature scaling during the transient startup period before reaching initial steady-state water flux, the ion concentrations were adjusted to 90 % of the actual composition. The feedwater pH was unadjusted and measured to be 7.05. The test solution simulates THBIP-pretreated RO feed by

maintaining the same ion concentrations as the control (i.e., 90 % of actual values) but with divalent Ca^{2+} and Mg^{2+} concentrations reduced by 33.0 % and 90.1 %, respectively. The reductions in hardness cations are based conservatively on the experimental results of our previous THBIP study, which achieved approximately 100 % Mg^{2+} removal and 33 % Ca^{2+} removal using diisopropylamine as the thermomorphic hydrophilicity base in a 4.0 mol/L NaCl brine containing 0.020 mol/L each of $CaCl_2$ and $MgCl_2$ (with amine dosage of 1.25 mol per L of feed, mixing temperature of 15 °C, demixing temperature of 70 °C, and equilibration time of 1 h; full details can be found in our previous publication) [33]. Ammonium was intentionally included to represent residual amine species (protonated) after regeneration of the basic amine in THBIP. Ion compositions of both feedwaters are listed in Table 1.

Permeate water flux, J_w, is defined as the permeate volumetric flowrate normalized by the active membrane area and is determined according to the procedures detailed in a previous study [36]. For the scaling experiments, J_w was continuously monitored at 10 s intervals using a data acquisition (DAQ) system throughout the experimental runs. Raw J_w was subsequently processed using 10 min moving averages to smooth out instrument noise while preserving transient scaling dynamics. Feed temperature was maintained at 20 ± 0.1 °C using a recirculating chiller system to prevent unintended supersaturation caused by temperature fluctuations. Water recovery yield, Y, is defined as the mass ratio of cumulative permeate to initial feedwater:

$$Y \equiv \frac{\sum m_p}{m_f} \tag{1}$$

where m is mass and subscripts p and f denote permeate and feed, respectively. Salt rejection, R, was evaluated through the percentage reduction in ionic conductivity of the permeate relative to the retentate (indicated by subscript r):

$$R = 1 - \frac{\sigma_p}{\sigma_r} \tag{2}$$

where σ is the ionic conductivity and was measured using a conductivity meter (STAR A212, ThermoFisher). Schematic of the RO experimental setup is illustrated in Fig. 1.

2.3. Water chemistry analysis of mineral precipitation potential

The thermodynamic driving force for mineral precipitation in the control and THBIP-pretreated feeds was analytically assessed using saturation indices computed through water chemistry modeling with Visual MINTEQ software (Uppsala, Sweden). Six mineral phases were evaluated: gypsum ($CaSO_4 \bullet 2H_2O$), anhydrite ($CaSO_4$), dolomite ($CaMg(CO_3)_2$), calcite (trigonal $CaCO_3$), aragonite (orthorhombic $CaCO_3$), and vaterite (hexagonal $CaCO_3$), which represent the primary scaling species of concern for the investigated feed compositions. To simplify the analysis, all ions were assumed to concentrate proportionally in the retentate with increasing water recovery yields, i.e., 100 % ion rejection, an assumption supported by the consistently high salt rejection of the BW30 membrane used in this study (NaCl: >99.4 %, $CaCl_2$: >99.4 %, and $MgSO_4$: >99.7 %) [37].

2.4. Characterization of scaling on reverse osmosis membrane

Surface morphology of scalant deposits on the membranes was characterized using high-resolution scanning electron microscopy, SEM (SIGMA VP, Carl Zeiss AG, Jena, Germany), at 10 kV accelerating voltage and with up to 5500× magnification. The SEM was coupled with energy-dispersive X-ray spectroscopy (EDS) for elemental composition mapping and quantitative analysis of deposit heterogeneity across membrane surfaces. Crystal identification and structural analysis of scalant deposits were performed using X-ray diffraction crystallography, XRD (Rigaku SmartLab diffractometer, Tokyo, Japan) with Cu Kα radiation (λ = 1.5418 Å). XRD spectra were collected across a 2θ range of 0° to 80° using a scanning rate of 0.02°/s to characterize both crystalline and amorphous phases within the scaling layers. The mineral precipitates were characterized by thermogravimetric analysis (TGA, Q500, TA instruments, New Castle, NY, United States) to categorize the scalant species and quantify their relative proportions. Free water was removed by storing the TGA samples in a vacuum oven at 35 °C. The TGA program was set to ramp from 20 °C to 200 °C in 10 min and then maintained at 200 °C for another 20 min. Additionally, cation species and concentrations of the solid scales were analyzed by inductively coupled plasma mass spectrometry (ICP-MS, 7900, Agilent Technologies, Santa Clara, CA, United States) after redissolving in dilute hydrochloric acid.

3. Results and discussion

3.1. THBIP pretreatment of reverse osmosis feed to reduce hardness

The working principles of thermomorphic hydrophilicity base-induced precipitation as a pretreatment for RO are illustrated in Fig. 2. Without THBIP or other pretreatments to mitigate the scaling precursor ions, feedwater containing high concentrations of hardness cations (typically Ca^{2+} and Mg^{2+}) is fed directly into the membrane modules (Fig. 2a). Ions are highly rejected by the RO membrane, with multivalent species almost completely excluded (99.4–99.7 %) [37]. This results in concentration polarization, where the rejected ion concentrations at the solution-membrane interface increase substantially, reaching 2–4× the bulk concentrations [16,38–42]. Because of the elevated concentrations of Ca^{2+}, Mg^{2+}, SO_4^{2-}, and CO_3^{2-}, the saturation limits of sparing soluble salts are exceeded and nucleation and crystallization are initiated, leading to the formation of mineral scalants on the membrane surface, i.e., scaling.

THBIP mitigates scaling in RO through pH-directed precipitation of magnesium and calcium salts from the feed using basic amines with thermally responsive solubility in water (Fig. 2b) [33]. Addition of the basic amine to the feed (at ambient temperature) significantly elevates solution pH (Step 1). The increased basicity induces precipitation of hardness cations as low-solubility mineral phases, primarily as calcium and magnesium hydroxides (Step 2). The precipitated mineral solids are removed by sieving (Step 3). While this pH-directed precipitation mechanism is achieved through amine addition, the amine is not consumed in the precipitation and can be recovered for reuse by utilizing the thermomorphic hydrophilicity behavior of the base. By warming the solution to moderate temperatures of 40–80 °C the amine undergoes a hydrophilic-to-hydrophobic transition [43,44], drastically lowering its solubility in water and driving spontaneous demixing (Step 4). The amine phase separates into a light organic phase while the

Table 1
Feed ion concentrations simulating untreated, i.e., raw feed, control, and THBIP-pretreated streams at the San Luis RO Plant.

	Ion concentrations (mg/L)							
	Na^+	Ca^{2+}	Mg^{2+}	NH_4^+	SO_4^{2-}	Cl^-	HCO_3^-	NO_3^-
Raw feed	3107	518	336	0	6121	2073	178	20
Control	2796	466	302	0	5509	1866	160	18
THBIP-pretreated	2796	312	30	541	5509	1866	160	18

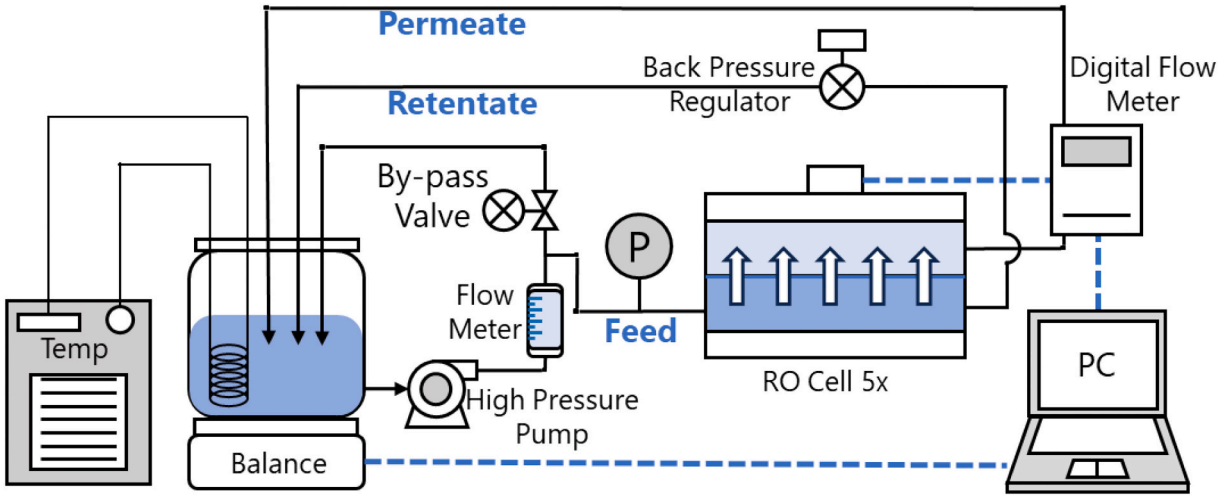

Fig. 1. Schematic of the bench-scale, crossflow RO setup for membrane scaling experiments. The high-pressure pump circulates the pressurized feedwater at 27.6 bar (400 psi) and 0.11 m/s. Permeate water flux was automatically logged to a computerized data acquisition system, and feed temperature is maintained at 20 ± 0.1 °C.

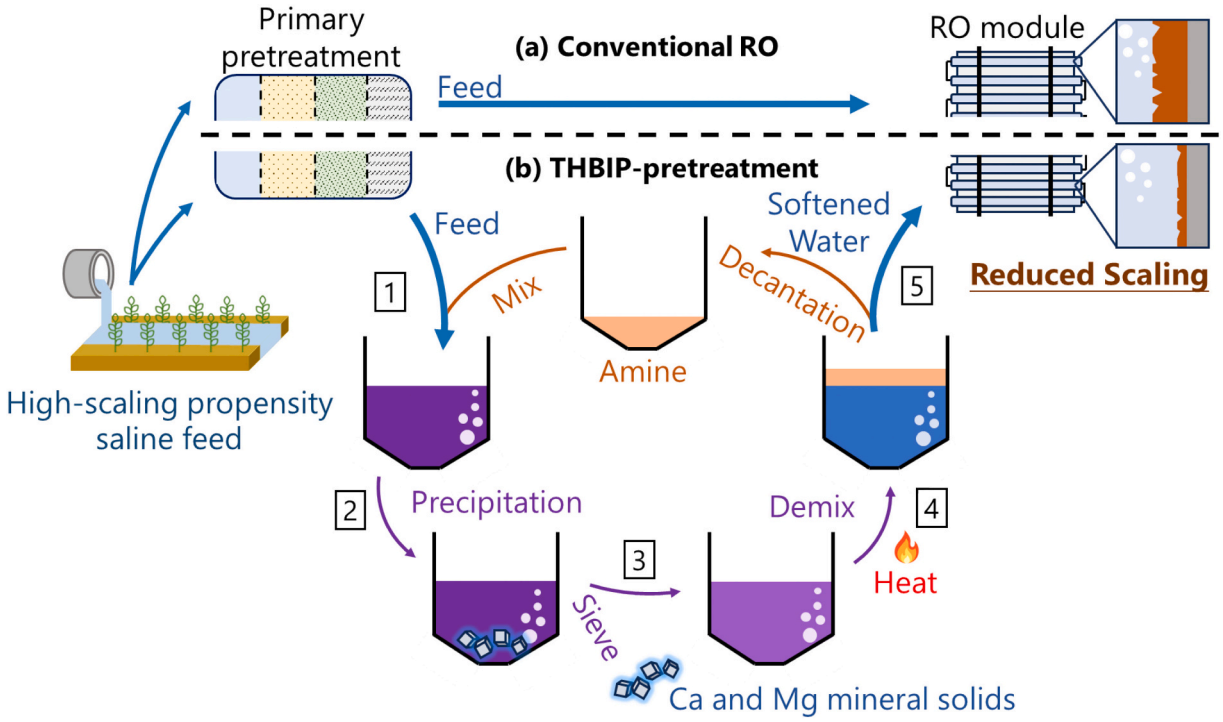

Fig. 2. Process schematic comparing RO (a) without and (b) with thermomorphic hydrophilicity base-induced precipitation (THBIP) pretreatment. THBIP reduces hardness cations concentrations through pH-directed precipitation using basic thermomorphic hydrophilicity amines that can be regenerated and reused. In THBIP pretreatment, the amine base is added to the high-scaling propensity feed to elevate the pH (Step 1) and induce precipitation of mineral solids (Step 2), which can be readily sieved out (Step 3). Hydrophilicity of the amine molecule is highly sensitive to temperature. Applying a mild heat stimulus drastically lowers amine polarity and causes the amine to demix from the aqueous brine feed (Step 4). The demixed amine forms a distinct immiscible liquid layer that can be physically separated, thus recovering the amine for subsequent reuse (Step 5). Membrane scaling in the subsequent RO is mitigated as hardness cations are removed.

descaled feedwater forms the heavy aqueous phase. The amine is readily removed and recovered from the biphasic mixture by physical separation, i.e., decantation, and recycled for the next THBIP precipitation cycle (after cooling back to ambient temperature), and the hardness-reduced feedwater is fed into the RO module (Step 5). Because the scaling precursor ions, such as Ca^{2+} and Mg^{2+}, had been removed from the feed by the THBIP pretreatment, membrane scaling is significantly reduced.

3.2. THBIP pretreatment mitigates membrane scaling to improve water recovery yield

Table 1 presents the untreated and THBIP-pretreated compositions simulating feedwaters at the San Luis RO Plant. The untreated concentrations of Ca^{2+} and Mg^{2+} are 466 and 302 mg/L, respectively. THBIP pretreatment selectively removes hardness ions, lowering Ca^{2+} and Mg^{2+} concentrations to 312 and 30 mg/L, corresponding to reductions of 33.0 % and 90.1 % [33]. The disparity between Ca^{2+} and Mg^{2+} removal is due to the difference in hydroxide solubility: less soluble Mg

$(OH)_2$ ($K_{sp} = 10^{-11.22}$) precipitates out almost completely from solution, but $Ca(OH)_2$ is considerably more soluble ($K_{sp} = 10^{-5.20}$) and, hence, Ca^{2+} is only partially removed by the pH elevation from THBIP (detailed quantitative analysis can be found in our previous study) [33]. The targeted precipitation of divalent cations by THBIP decreased overall hardness by 55.4 %, whereas total dissolved solids remained unchanged [33].

The impact of THBIP hardness removal on membrane scaling mitigation was quantified by analyzing normalized water flux, $J_w/J_{w,0}$ (relative to time = 0) as a function of water recovery yield, Y (Fig. 3a). As the osmotic pressure is essentially unchanged, $J_{w,0}$ of the control and THBIP-pretreated feeds are almost identical (46.3 Lm^{-2} h^{-1} and 44.1 Lm^{-2} h^{-1} for the two runs, compared to 43.5 Lm^{-2} h^{-1} and 40.9 Lm^{-2} h^{-1}, respectively; marginal differences are due to inherent variability of water permeance between membrane coupons), thus eliminating the potential effects of advective water transport on fouling [45,46]. The control experimental runs exhibited a characteristic flux decline trajectory (green hexagon and square symbols; hereafter, the terms "flux decline", "flux deterioration", and "flux decay" are used interchangeably to describe the gradual decrease in water flux as a function of time), with an initial gradual water permeability reduction followed by a sharp flux deterioration beyond a critical point. For the untreated feeds, the transition from gradual to rapid J_w decline occurred at $Y \approx 0.5$. In one of the control runs, J_w effectively vanished at around Y of 0.65 (the other control run was terminated before $J_w \rightarrow 0$).

The gradual J_w decline is partly attributed to the progressive reduction in net driving force for water flux. Because salts are highly rejected by the RO membrane ($R > 99.4$ %), the feed osmotic pressure steadily rises with the water recovery yield; for instance, osmotic pressure is approximately doubled at $Y = 0.5$. As the net driving force for water flux is the applied hydraulic pressure (maintained constant in all experiments) minus the feed osmotic pressure, J_w should decrease with increasing Y. However, quantitative analysis of effect of Y on the net driving force reveals that the expected flux decay cannot fully account for the observed decline in $J_w/J_{w,0}$ of Fig. 3a, indicating that mild fouling of the membrane is already occurring before $Y = 0.5$, likely due to scaling driven by concentration polarization at the solution-membrane interface [24,27]. The abrupt acceleration in water flux decline at $Y \approx 0.5$ suggests the onset of scaling by bulk precipitation of supersaturated minerals [24,27]. Analysis of the saturation indices will be discussed later.

Scaling mitigation by THBIP pretreatment of the RO feeds is evident from the water flux profiles of Fig. 3a (red circle and diamond symbols). To more accurately quantify the critical transition point of water flux decline, piecewise linear regression analysis was applied using Python to identify the inflection points and determine the slopes. Firstly, $J_w/J_{w,0}$ decline rate during the initial scaling (i.e., gradual slope) is lower than the untreated control (slopes of −0.64 and −0.75, respectively). Again, the progressive increase in feed osmotic pressure cannot fully explain the water flux decay. Secondly, THBIP pretreatment delayed the critical transition from $Y = 0.48$ point to 0.61, representing a 27 % enhancement in achievable recovery before water flux declined more intensively. Thirdly, water flux decline after the transition to the more severe membrane scaling is drastically lessened in the THBIP-pretreated feed compared to the control ($J_w/J_{w,0}$-Y slopes of −2.9 and −10.1, respectively), which represents a 71.7 % reduction. The pretreatment enabled

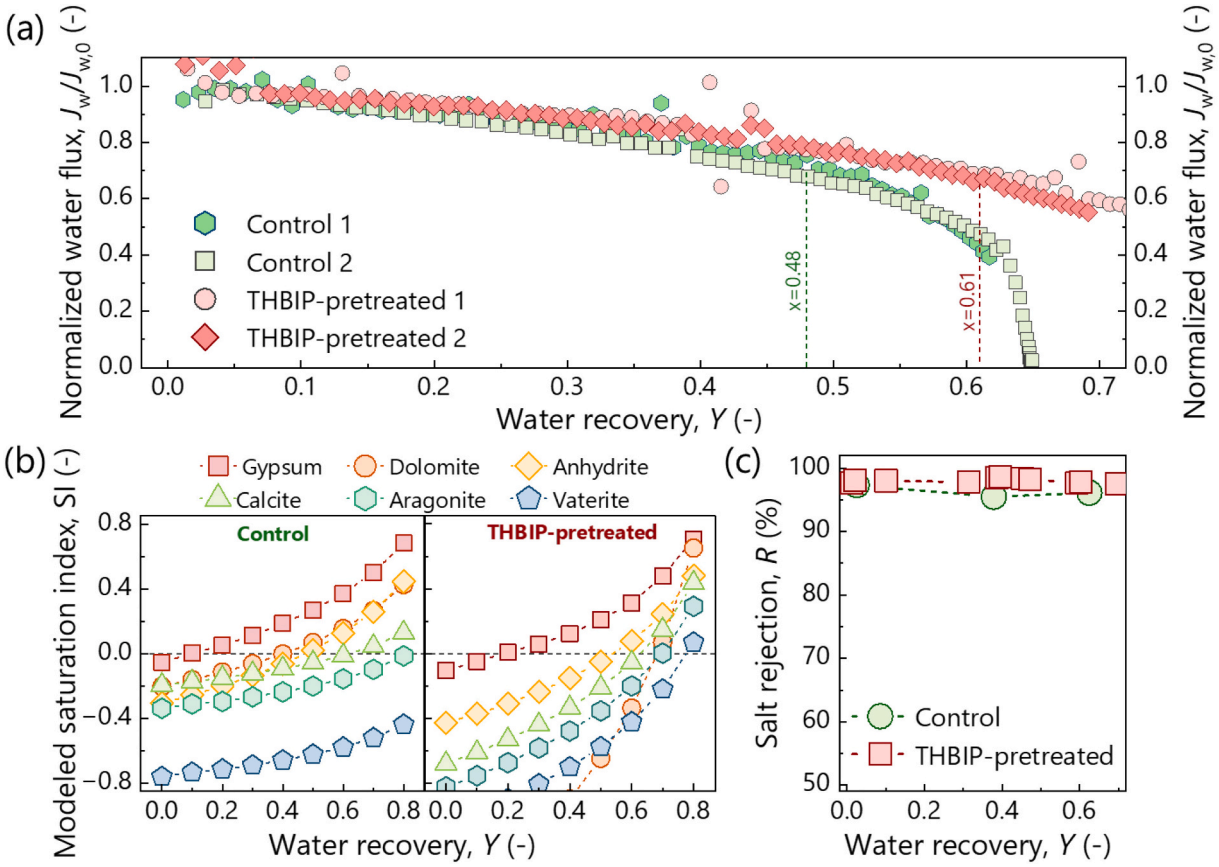

Fig. 3. (a) Normalized water flux, $J_w/J_{w,0}$, profiles as a function of water recovery yield, Y, for two controls runs (green hexagon and square symbols) and two THBIP-pretreated runs (red circle and diamond symbols). (b) Modeled saturation indices (SI) as a function of Y for the untreated and THBIP-pretreated feeds using Visual MINTEQ. Mineral phases analyzed are gypsum ($CaSO_4 \cdot 2H_2O$), dolomite ($CaMg(CO_3)_2$), anhydrite ($CaSO_4$), calcite (trigonal $CaCO_3$), aragonite (orthorhombic $CaCO_3$), and vaterite (hexagonal $CaCO_3$). Horizontal grey dotted line represents the saturation threshold (i.e., SI = 0), above which the mineral is supersaturated. (c) Salt rejection, R, sampled during the runs for the two experimental configurations.

water recovery yields beyond 0.70 while maintaining 55 % of initial water permeability. These provide compelling evidence that hardness removal by THBIP can significantly mitigate scaling.

Amine regeneration by application of a mild heat stimulus (i.e., Steps 4 and 5 of Fig. 2) was demonstrated in our previous study [33]. Because the thermomorphic bases are also volatile, residual THBIP amines remaining in the feed can be further recovered by air stripping [47,48]. A basic laboratory air stripping experiment was conducted and achieved up to 92.3 % regeneration efficiency (after a THBIP cycle with diisopropylamine, air was bubbled through the feed at 6 L/min for 1 h); higher amine recovery efficiencies can be attained with an optimally designed air stripping unit operation. Residual amines remaining in the feed that are not recovered are expected to have negligible effect on RO. Following the demixing step of THBIP and air stripping, the feed pH is lowered to 9.68, within the membrane operating pH range of 2–11. The polyamide chemistry of thin-film composite RO membranes is not known to have significant reactions with amines. Our previous study evaluated rejection of the THBIP amines by RO and achieved consistently high rejection, signifying that the active layer integrity is not compromised [33].

3.3. Saturation index analysis reveals that gypsum and anhydrite are the principal scalants

Thermodynamic speciation modeling using saturation indices (SI) identified predominant scaling species across the investigated range of water recovery yields, assuming perfect rejection of all ions (Fig. 3b). Note that although the analysis does not factor in concentration polarization and is, hence, more representative of the bulk solution environment, the results can nonetheless provide qualitative indications of the scaling happening at the solution-membrane interface. For both untreated and THBIP-pretreated feeds, gypsum, $CaSO_4{\cdot}2H_2O$ (red square symbols), exhibited the highest supersaturation levels for all Y, with SI > 0 immediately upon initiation of the RO runs. Thus, the initial gradual flux decline observed in both operations can be explained by localized gypsum precipitation, consistent with findings of previous studies [49]. In the controls, the critical scaling transition (i.e., drastic change in dJ_w/dY) at $Y = 0.48$ from the experimental water flux profiles coincided with the SIs for anhydrite and dolomite turning positive at $Y \approx 0.5$ ($CaSO_4$ and $CaMg(CO_3)_2$; yellow diamond and orange circle symbols, respectively). The delayed inflection point at 0.61 in the THBIP-pretreated feed aligned with the supersaturation of anhydrite. Therefore, anhydrite is the most probable culprit for membrane scaling through precipitation in the bulk solution phase. Although dolomite was also supersaturated in the controls, precipitation of the mineral at ambient temperatures is unlikely due to kinetic barriers associated with the crystal growth process [50].

Salt rejection, R, was evaluated by characterizing ionic conductivities of the permeates and retentates at different points during the experimental runs (Fig. 3c). Both experimental configurations achieved similarly high salt rejections throughout, signifying that the membrane selectivity is preserved despite the scaling.

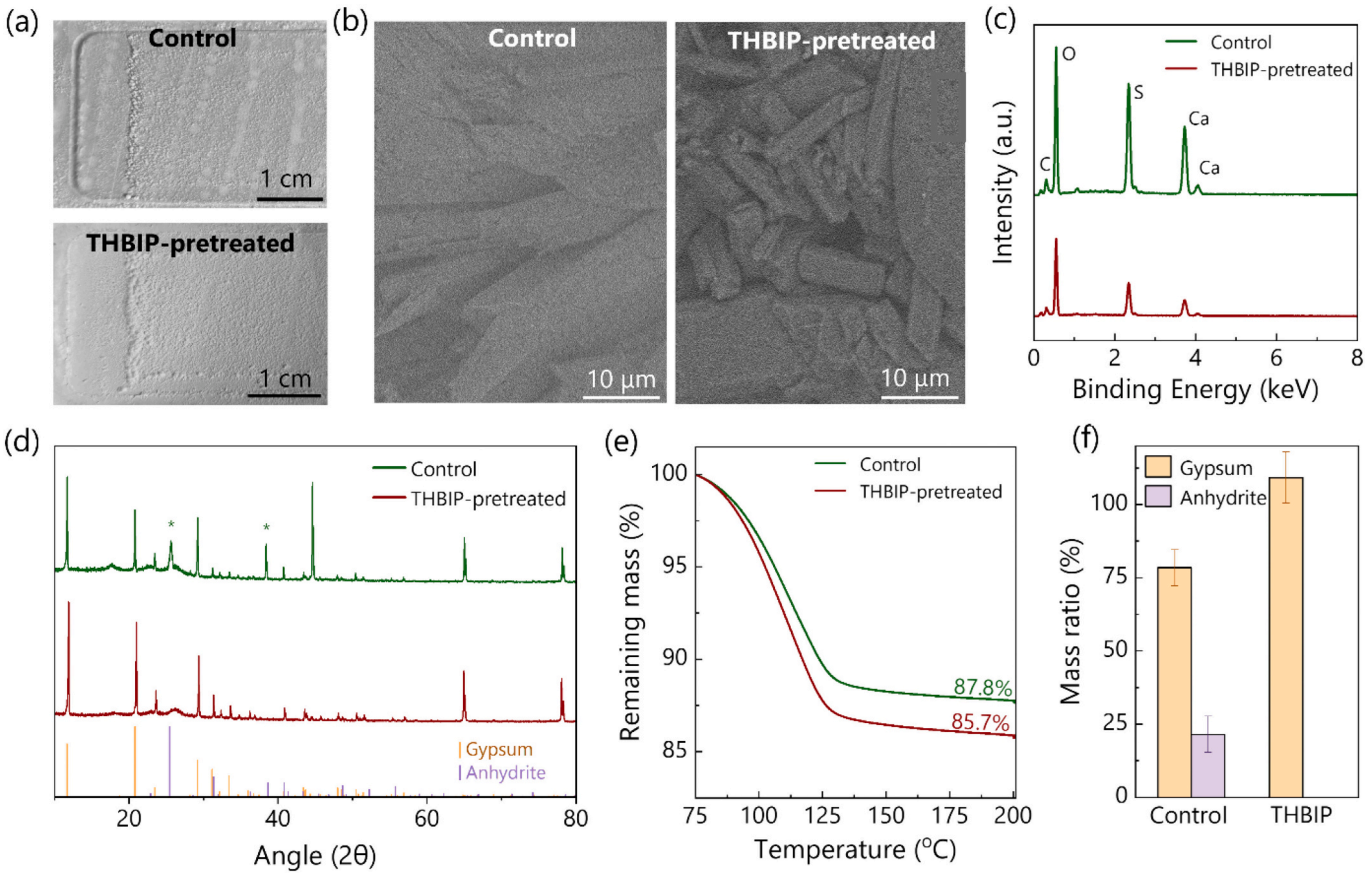

Fig. 4. (a) Photographic images and (b) SEM micrographs of scalants on control and THBIP-pretreated membranes after RO scaling experiments. (c) EDS spectra across the binding energies for carbon, oxygen, magnesium, sulfur, and calcium and (d) XRD intensity as a function of diffraction angle for the scalant deposits on control and THBIP-pretreated membranes (green and red lines, respectively). Orange and violet vertical lines correspond to reference XRD spectra for gypsum and anhydrite. (e) Thermogravimetric analysis (TGA) profiles showing scalant mass of control and THBIP-pretreated samples as a function of temperature. (f) Gypsum and anhydrite mass ratios of mineral scales from control and THBIP-pretreated membranes determined using ICP-MS Ca^{2+} concentrations and masses of the redissolved solids. Data points and error bars are means and standard errors, respectively, of triplicate samples.

3.4. Membrane scaling is suppressed by THBIP pretreatment through delaying anhydrite formation

Post-scaling characterization was conducted to evaluate differences in scalant characteristics and morphology between control and THBIP-pretreated membranes. Rough layers of opaque white solids were observed on both membrane surfaces, with more pronounced imprints of rectangular compression patterns on the control indicating formation of thicker scaling layers compared to THBIP-pretreated membranes (Fig. 4a). This is consistent with the above water flux analysis (Fig. 3a). High-resolution scanning electron microscopy revealed crystalline deposits characterized by predominantly acicular habits (needle-like structures) for both membrane surfaces (Fig. 4b). On the control membrane, elongated needles ≈30–50 nm in length signified mature crystal growth under sustained supersaturated conditions [21,51]. In contrast, THBIP-pretreated membranes had significantly smaller crystals with dimensions of ≈5–15 nm. The morphological features are consistent with gypsum ($CaSO_4{\cdot}2H_2O$) and anhydrite ($CaSO_4$), common inorganic scalants in seawater RO [52–54].

Energy-dispersive X-ray spectroscopy (EDS) confirmed calcium, sulfur, and oxygen as the primary elements of the scalants with negligible magnesium for both control and THBIP-pretreated membranes, thus excluding dolomite formation and corroborating $CaSO_4$ as the chemical formula of the scalant (Fig. 4c). X-ray diffraction (XRD) crystallography further validated these findings, with both membrane surfaces exhibiting diffraction patterns consistent with standard gypsum spectra (Fig. 4d) [52,53]. Sharper diffraction peaks in the control indicate more ordered crystalline structures, attributed to extended growth periods and increased deposit thickness. Distinct diffraction peaks at $2\theta = 25.6^\circ$ and 38.4° (marked by asterisks in Fig. 4d) are characteristic of anhydrite and were observed exclusively in the control, confirming significant anhydrite formation alongside gypsum.

The morphological, elemental, and crystallographic analyses of Fig. 4 align closely with the saturation index modeling in Fig. 3b, together providing a coherent explanation of the observed flux decline in Fig. 3a. The two approaches independently determined gypsum precipitation to be causing the initial gradual flux decay in both control and THBIP-pretreated membranes. The steeper slope of flux decline in the control is explained by the formation of thicker deposits with larger, more ordered crystals. Anhydrite forms denser, less permeable deposits than gypsum [55,56]. Both analyses found that the subsequent onset of anhydrite saturation and precipitation in the control experiments marks the critical transition to accelerated flux loss. In contrast, the absence of distinct anhydrite peaks in the XRD spectra of THBIP-pretreated membranes signals that formation of this dense scalant phase is limited and accounts for the substantially milder flux decline.

TGA analysis showed that after heating to 200 °C, 87.8 % and 85.7 % of the mass remained in the control and THBIP-pretreated samples, respectively (Fig. 4e, 75 °C as baseline). The mass loss is attributed to hydrating water vaporizing from gypsum [57]: $CaSO_4{\cdot}2H_2O \xrightarrow{\Delta} CaSO_4{\cdot}0.5H_2O + 1.5H_2O$. Utilizing the water mass ratio derived from the TGA results, gypsum was determined to account for 91.2 % of the total solid mass in the THBIP-pretreated sample, compared to 77.2 % in the control sample (assuming gypsum, $CaSO_4{\cdot}2H_2O$, and anhydrite, $CaSO_4$, are the only initial constituents), i.e., 22.8 % of the control sample mass is anhydrite. ICP-MS analysis of the redissolved scalants confirmed, as expected, the absence of dolomite in the solid phase (negligible Mg^{2+} concentrations in all samples). Assuming that only gypsum and anhydrite are contributing to the measured Ca^{2+}, the relative proportion of the two minerals can be determined by comparing the measured concentration to the actual redissolved mass. As shown in Fig. 4f, scalants on the control membrane comprise 77.4 ± 7.2 % gypsum and 21.1 ± 5.8 % anhydrite, whereas the THBIP-pretreated membrane effectively had only gypsum. The inexact match between TGA and ICP-MS results is ascribed to the different experimental approaches, but both methods qualitatively agree and corroborate that THBIP pretreatment can suppress anhydrite scaling.

Although $CaSO_4{\cdot}2H_2O$ remained the predominant scalant species, THBIP-pretreatment significantly retarded initial gypsum precipitation and drastically impeded the formation and accumulation of anhydrite, the secondary but denser scalant. Overall, pretreatment of the feed by THBIP extended the operational window for adequate water flux, thus enhancing RO productivity for the desalination of high-scaling propensity feeds.

4. Conclusion

This investigation demonstrates that pretreatment of high-scaling propensity feeds by thermomorphic hydrophilicity base-induced precipitation (THBIP) markedly suppresses water flux decline caused by scaling to enhance reverse osmosis performance. By integrating thermodynamic, morphological, elemental, and crystallographic analyses, we conclusively showed that gypsum was the initial foulant, whereas the subsequent onset of anhydrite saturation triggered the critical transition to severe scaling and accelerated water flux loss. Removing hardness cations from the simulated irrigation drainage water using THBIP pushed back this critical scaling transition (from water recovery yield of 0.48 to 0.61), considerably extending the operational window for water production (by 27 %). The targeted removal of divalent cations—particularly 30 % of Ca^{2+}—mitigated catastrophic flux collapse caused by anhydrite scaling. The permanent hardness removal coupled with pH rebalancing through amine recovery by application of a thermal stimulus fundamentally differentiates THBIP from other scaling mitigation approaches, such as lime softening and antiscalant complexation. The pH reversion further eliminates additional neutralization costs. The scaling mitigation demonstrated here was achieved without further optimization of the THBIP parameters and performance beyond the original study. Thus, there is substantial potential for improving Ca^{2+} removal through the thoughtful selection of alternative thermomorphic amine bases with lower pK_b and enhanced aqueous solubility. Future studies can investigate the effectiveness of THBIP on mitigating potential synergistic scaling from silica co-precipitation and assess performance of the technique with more complex feedwaters containing multiple scaling precursors beyond Ca^{2+} and Mg^{2+}, including in module-scale systems. THBIP presents straightforward scalability due to the relative ease of operation and use of commodity chemicals. The unique combination of amine recyclability, feed pH rebalancing (after amine separation), and compatibility with low-grade heat utilization positions THBIP as a more effective and sustainable alternative for descaling desalination feeds and hypersaline brines, enabling fit-for-purpose reuse, enhanced water recovery, and even zero-liquid discharge.

CRediT authorship contribution statement

Yuren Feng: Writing – original draft, Visualization, Methodology, Investigation, Formal analysis, Data curation, Conceptualization. **Sara Abu-Obaid:** Writing – review & editing, Investigation, Formal analysis. **Daniel Galperin:** Methodology, Investigation, Formal analysis, Data curation, Conceptualization. **Ngai Yin Yip:** Writing – review & editing, Supervision, Funding acquisition, Formal analysis, Conceptualization.

Funding sources

This material is based upon work supported by the U.S. Bureau of Reclamation under Grant No. R19AC00111. Any opinions, findings, and conclusions or recommendations expressed in this material are those of the author(s) and do not necessarily reflect the views of the Bureau of Reclamation.

Declaration of competing interest

The authors declare the following financial interests/personal relationships which may be considered as potential competing interests: Ngai Yin Yip reports financial support was provided by Columbia University. Ngai Yin Yip has patent issued to Columbia University. If there are other authors, they declare that they have no known competing financial interests or personal relationships that could have appeared to influence the work reported in this paper.

Acknowledgments

The authors thank Dr. Miguel Arias-Paic for guidance on the water chemistry of feedwater at the San Luis reverse osmosis facility. The authors acknowledge the use of facilities and instrumentation supported by the National Science Foundation through the Columbia University, Columbia Nano Initiative, and the Materials Research Science and Engineering Center DMR-2011738.

Data availability

Data will be made available on request.

References

[1] E.R. Jones, M.F.P. Bierkens, M.T.H. van Vliet, Current and future global water scarcity intensifies when accounting for surface water quality, Nat. Clim. Chang. 14 (6) (2024) 629–635, https://doi.org/10.1038/s41558-024-02007-0.
[2] C. He, Z. Liu, J. Wu, X. Pan, Z. Fang, J. Li, B.A. Bryan, Future global urban water scarcity and potential solutions, Nat. Commun. 12 (1) (2021) 4667, https://doi.org/10.1038/s41467-021-25026-3.
[3] M.M. Mekonnen, A.Y. Hoekstra, Four billion people facing severe water scarcity, Sci. Adv. 2 (2) (2016) e1500323, https://doi.org/10.1126/sciadv.1500323.
[4] FAO and UN Water (Ed.), Progress on the Level of Water Stress, 2021, https://doi.org/10.4060/cb6241en.
[5] P. Greve, T. Kahil, J. Mochizuki, T. Schinko, Y. Satoh, P. Burek, G. Fischer, S. Tramberend, R. Burtscher, S. Langan, Y. Wada, Global assessment of water challenges under uncertainty in water scarcity projections, Nat. Sustain. 1 (9) (2018) 486–494, https://doi.org/10.1038/s41893-018-0134-9.
[6] P. Ghosal, S. Sahu, H. Patel, P.S. Ghosal, A comprehensive review on desalination using membrane-based technologies in India: a bibliometric analysis and meta-analysis, Desalination 598 (2025) 118418, https://doi.org/10.1016/j.desal.2024.118418.
[7] A. Shabib, B. Tatan, Y. Elbaz, A. Aly Hassan, M.A. Hamouda, M.A. Maraqa, Advancements in reverse osmosis desalination: technology, environment, economy, and bibliometric insights, Desalination 598 (2025) 118413, https://doi.org/10.1016/j.desal.2024.118413.
[8] W. Yuan, X. Chen, Z. Yu, Y. Wan, J. Lin, W. Ye, Critical review of membrane fouling in reverse osmosis treatment: characterizations, models, mechanisms, and controls, Sep. Purif. Technol. 363 (2025) 132119, https://doi.org/10.1016/j.seppur.2025.132119.
[9] J. Li, W. Cheng, H. Wang, Y. Luo, Q. Liu, X. Wang, L. Wang, T. Zhang, Reverse osmosis and nanofiltration processes in industrial wastewater treatment: the recent progress, challenge, and future opportunity, Sep. Purif. Technol. 362 (2025) 131687, https://doi.org/10.1016/j.seppur.2025.131687.
[10] Y. Kim, G. Lee, J. Byun, S. Lim, S. Lee, Y.-G. Park, Optimizing energy efficiency in desalination: performance evaluation of seawater reverse osmosis and pressure retarded osmosis hybrid systems, Desalination 601 (2025) 118557, https://doi.org/10.1016/j.desal.2025.118557.
[11] J. Shen, X. Wang, X. Zhu, B. Tang, C. Liu, W. Li, X. Gao, Scaling in reverse osmosis seawater desalination: mechanism and prevention—a literature review, Can. J. Chem. Eng. 103 (2) (2025) 503–523, https://doi.org/10.1002/cjce.25427.
[12] J. Li, W. Cheng, H. Wang, Y. Luo, Q. Liu, X. Wang, L. Wang, T. Zhang, Reverse osmosis and nanofiltration processes in industrial wastewater treatment: the recent progress, challenge, and future opportunity, Sep. Purif. Technol. 362 (2025) 131687, https://doi.org/10.1016/j.seppur.2025.131687.
[13] S. Ouali, A. Doucoure, Adopting sea water reverse osmosis desalination technologies for sustainable development: lessons learnt from Algiers Science and Technology for Membranes 2023 workshop, Front. Membr. Sci. Technol. 3 (2024), https://doi.org/10.3389/frmst.2024.1352799.
[14] E.W. Tow, Q.J. Wei, A.R. Abraham, K.L. Chua, M.J. Plumley, J.H. Lienhard, Piloting batch reverse osmosis with a flexible bladder for water recovery from scaling-prone brine, NPJ Clean Water 8 (1) (2025) 30, https://doi.org/10.1038/s41545-025-00462-6.
[15] G.L.D. Pereira, V. Jegatheesan, Mapping the evolution of seawater desalination research (2000–2024): bibliometric and Co-word analysis of 11,000+ publications, Desalination 591 (2024) 118029, https://doi.org/10.1016/j.desal.2024.118029.
[16] A.J. Karabelas, S.T. Mitrouli, M. Kostoglou, Scaling in reverse osmosis desalination plants: a perspective focusing on development of comprehensive simulation tools, Desalination 474 (2020) 114193, https://doi.org/10.1016/j.desal.2019.114193.
[17] K.M. Shah, I.H. Billinge, X. Chen, H. Fan, Y. Huang, R.K. Winton, N.Y. Yip, Drivers, challenges, and emerging technologies for desalination of high-salinity brines: a critical review, Desalination 538 (2022) 115827, https://doi.org/10.1016/j.desal.2022.115827.
[18] Y. Kim, J. Byun, K. Park, Y.-G. Park, Comprehensive analysis of energy saving and high-quality permeate production strategies for a large-scale seawater reverse osmosis desalination plant with diverse process configurations and external resource utilization, Desalination 596 (2025) 118292, https://doi.org/10.1016/j.desal.2024.118292.
[19] T. Tong, S. Park, Y. Yao, A tale of two minerals: contrasting behaviors and mitigation strategies of gypsum scaling and silica scaling in membrane desalination, Front. Environ. Sci. Eng. 19 (1) (2024) 3, https://doi.org/10.1007/s11783-025-1923-9.
[20] Y. Chen, Y. Cohen, Calcium sulfate and calcium carbonate scaling of thin-film composite polyamide reverse osmosis membranes with surface-tethered polyacrylic acid chains, Membranes 12 (12) (2022) 1287, https://doi.org/10.3390/membranes12121287.
[21] S. Park, M. Saavedra, X. Liu, T. Li, B. Anger, T. Tong, A comprehensive study on combined organic fouling and gypsum scaling in reverse osmosis: decoupling surface and bulk phenomena, J. Membr. Sci. 694 (2024) 122399, https://doi.org/10.1016/j.memsci.2023.122399.
[22] M. Jebur, Y.-H. Chiao, H. Matsuyama, S.R. Wickramasinghe, Electrocoagulation as a pretreatment for reverse osmosis for potable water from brackish groundwater, Water Resour. Ind. 31 (2024) 100243, https://doi.org/10.1016/j.wri.2024.100243.
[23] L.F. Greenlee, D.F. Lawler, B.D. Freeman, B. Marrot, P. Moulin, Reverse osmosis desalination: water sources, technology, and today's challenges, Water Res. 43 (9) (2009) 2317–2348, https://doi.org/10.1016/j.watres.2009.03.010.
[24] Y.M. Al-Roomi, K.F. Hussain, Potential kinetic model for scaling and scale inhibition mechanism, Desalination 393 (2016) 186–195, https://doi.org/10.1016/j.desal.2015.07.025.
[25] Y. Xiao, K. Chen, M. Sun, P. Xiong, B. Huang, Y. Sun, D. Chen, J. Gan, Z. Yang, Synergy between defects and lattice distortion drives self-powered elastico-near-infrared mechanoluminescence in Cr3+-doped spinel oxides, Adv. Sci. 12 (39) (2025) e10848, https://doi.org/10.1002/advs.202510848. October 20.
[26] W. Yu, W. Chen, H. Yang, Evaluation of structural effects on the antiscaling performance of various graft cellulose-based antiscalants in RO membrane scaling control, J. Membr. Sci. 620 (2021) 118893, https://doi.org/10.1016/j.memsci.2020.118893.
[27] A. Antony, J.H. Low, S. Gray, A.E. Childress, P. Le-Clech, G. Leslie, Scale formation and control in high pressure membrane water treatment systems: a review, J. Membr. Sci. 383 (1) (2011) 1–16, https://doi.org/10.1016/j.memsci.2011.08.054.
[28] Z. Zeng, A. Sadeghpour, Y.S. Ju, A highly effective multi-string humidifier with a low gas stream pressure drop for desalination, Desalination 449 (2019) 92–100, https://doi.org/10.1016/j.desal.2018.10.017.
[29] D.A. Musale, B.B.J. Yao, S. Lopes, A. Urmenyi, M. Fazel, H. Lohokare, R. Yeleswarapu, A. Hallsby, A. Sheikh, A new phosphorous-free Antiscalant for membrane desalination, Desalin. Water Treat. 31 (1) (2011) 279–284, https://doi.org/10.5004/dwt.2011.2348.
[30] X. Li, D. Hasson, R. Semiat, H. Shemer, Intermediate concentrate demineralization techniques for enhanced brackish water reverse osmosis water recovery – a review, Desalination 466 (2019) 24–35, https://doi.org/10.1016/j.desal.2019.05.004.
[31] C.J. Gabelich, A. Rahardianto, C.R. Northrup, T.I. Yun, Y. Cohen, Process evaluation of intermediate chemical demineralization for water recovery enhancement in production-scale brackish water desalting, Desalination 272 (1) (2011) 36–45, https://doi.org/10.1016/j.desal.2010.12.050.
[32] C.J. Gabelich, M.D. Williams, A. Rahardianto, J.C. Franklin, Y. Cohen, High-recovery reverse osmosis desalination using intermediate chemical demineralization, J. Membr. Sci. 301 (1) (2007) 131–141, https://doi.org/10.1016/j.memsci.2007.06.007.
[33] C. Boo, H. Qi, I.H. Billinge, K.M. Shah, H. Fan, N.Y. Yip, Thermomorphic hydrophilicity base-induced precipitation for effective descaling of hypersaline brines, ACS EST Eng. 1 (9) (2021) 1351–1359, https://doi.org/10.1021/acsestengg.1c00160.
[34] E. Neofotistou, K.D. Demadis, Use of antiscalants for mitigation of silica (SiO2) fouling and deposition: fundamentals and applications in desalination systems, Desalination 167 (2004) 257–272, https://doi.org/10.1016/j.desal.2004.06.135.
[35] X. Tang, H. Liu, Mechanisms of alleviating gypsum scaling by antiscalants during membrane desalination: implications on agricultural drainage water reuse, ACS EST Water 4 (8) (2024) 3486–3494, https://doi.org/10.1021/acsestwater.4c00298.
[36] Y. Mo, A. Tiraferri, N.Y. Yip, A. Adout, X. Huang, M. Elimelech, Improved antifouling properties of polyamide nanofiltration membranes by reducing the density of surface carboxyl groups, Environ. Sci. Technol. 46 (24) (2012) 13253–13261, https://doi.org/10.1021/es303673p.
[37] Dupont FilmTec Co., Filmtec Reverse Osmosis Membranes Technical Manual, Version 18, https://www.dupont.com/content/dam/water/amer/us/en/water/public/documents/en/RO-NF-FilmTec-Manual-45-D01504-en.pdf#page=1.00, 2025.
[38] Y. Chen, Y. Cohen, Calcium sulfate and calcium carbonate scaling of thin-film composite polyamide reverse osmosis membranes with surface-tethered

polyacrylic acid chains, Membranes 12 (12) (2022) 1287, https://doi.org/10.3390/membranes12121287.
[39] S.S. Shenvi, A.M. Isloor, A.F. Ismail, A review on RO membrane technology: developments and challenges, Desalination 368 (2015) 10–26, https://doi.org/10.1016/j.desal.2014.12.042.
[40] M. Prisciandaro, V. Innocenzi, F. Tortora, G. Mazziotti di Celso, Reduction of fouling and scaling by calcium ions on an UF membrane surface for an enhanced water pre-treatment, Water 11 (5) (2019) 984, https://doi.org/10.3390/w11050984.
[41] M.D. Armstrong, R. Vickers, O. Coronell, Trends and errors in reverse osmosis membrane performance calculations stemming from test pressure and simplifying assumptions about concentration polarization and solute rejection, J. Membr. Sci. 660 (2022) 120856, https://doi.org/10.1016/j.memsci.2022.120856.
[42] O. Jung, F. Saravia, M. Wagner, S. Heißler, H. Horn, Quantifying concentration polarization – Raman microspectroscopy for in-situ measurement in a flat sheet cross-flow nanofiltration membrane unit, Sci. Rep. 9 (1) (2019) 15885, https://doi.org/10.1038/s41598-019-52369-1.
[43] R.T. Berry, E. Dach, J.A. Melhorn, N.Y. Yip, L. Soh, Assessing the temperature-dependent tunable polarity of N,N-dimethylcyclohexylamine (DMCHA) and water mixtures, ACS Sustain. Chem. Eng. 10 (11) (2022) 3726–3734, https://doi.org/10.1021/acssuschemeng.2c00293.
[44] E. Dach, E. Pisacane, D. Campbell, L. Soh, N.Y. Yip, Probing polarity structure–function relationships in amine–water mixtures, Chem. Commun. 61 (July 2025) 12988–12991, https://doi.org/10.1039/D5CC03314D.
[45] R.W. Field, G.K. Pearce, Critical, sustainable and threshold fluxes for membrane filtration with water industry applications, Adv. Colloid Interf. Sci. 164 (1) (2011) 38–44, https://doi.org/10.1016/j.cis.2010.12.008.
[46] R.W. Baker, Membrane Technology and Applications, Wiley, Hoboken, NJ, 2024.
[47] D.W. Green, M.Z. Southard (Eds.), Perry's Chemical Engineers' Handbook, 9th edition, McGraw-Hill Education, 2019.
[48] J.D. Seader, E.J. Henley, D.K. Roper, Separation process principles: With applications using process simulators, John Wiley & Sons, 2016.
[49] Y.-H. Chiao, M. Hu, R.R. Gonzales, Z. Yang, H. Matsuyama, Gypsum scaling behavior of the tannic acid-coated polyamide reverse osmosis membrane, ACS EST Water 4 (1) (2024) 237–244, https://doi.org/10.1021/acsestwater.3c00568.
[50] Y. Yin, T. Li, K. Zuo, X. Liu, S. Lin, Y. Yao, T. Tong, Which surface is more scaling resistant? A closer look at nucleation theories for heterogeneous gypsum nucleation in aqueous solutions, Environ. Sci. Technol. 56 (22) (2022) 16315–16324, https://doi.org/10.1021/acs.est.2c06560.
[51] C. Jia, G. Zhu, B.A. Legg, B. Guan, J.J. De Yoreo, Bassanite grows along distinct coexisting pathways and provides a low energy interface for gypsum nucleation, Cryst. Growth Des. 22 (11) (2022) 6582–6587, https://doi.org/10.1021/acs.cgd.2c00794.
[52] X. Qian, M. Ostwal, A. Asatekin, G.M. Geise, Z.P. Smith, W.A. Phillip, R.P. Lively, J. R. McCutcheon, A critical review and commentary on recent progress of additive manufacturing and its impact on membrane technology, J. Membr. Sci. 645 (2022) 120041, https://doi.org/10.1016/j.memsci.2021.120041.
[53] B. Maestracci, S. Delchini, D. Chateigner, H. Pilliere, L. Lutterotti, E. Borovin, Simultaneous combined XRF-XRD analysis of geological sample: new methodological approach for on-site analysis on new-Caledonian Ni-rich harzburgite, J. Geochem. Explor. 252 (2023) 107250, https://doi.org/10.1016/j.gexplo.2023.107250.
[54] S.Z. Ansari, A.B. Pandit, Evaluation of gypsum (CaSO4·2H2O) scale formation and its inhibition by different antiscalants by static and dynamic test, Indian Chem. Eng. 62 (3) (2020) 251–262, https://doi.org/10.1080/00194506.2019.1658547.
[55] P. Doubra, A. Kamran-Pirzaman, A.H. Mohammadi, R. Hassanalizadeh, Thermodynamic modelling of scale (calcite, barite, anhydrite and gypsum) deposition from brine, J. Mol. Liq. 230 (2017) 96–103, https://doi.org/10.1016/j.molliq.2016.11.135.
[56] K. Serafeimidis, G. Anagnostou, The solubilities and thermodynamic equilibrium of anhydrite and gypsum, Rock Mech. Rock. Eng. 48 (1) (2015) 15–31, https://doi.org/10.1007/s00603-014-0557-1.
[57] F. Paulik, J. Paulik, M. Arnold, Thermal decomposition of gypsum, Thermochim. Acta 200 (1992) 195–204, https://doi.org/10.1016/0040-6031(92)85115-C.